

Propeller-Like Nanorod-Upconversion Nanoparticle Assemblies with Intense Chiroptical Activity and Luminescence Enhancement in Aqueous Phase

Xiaoling Wu, Liguang Xu, Wei Ma, Liqiang Liu, Hua Kuang,* Nicholas A. Kotov, and Chuanlai Xu

Chiral assemblies are currently one of the most dynamic research fields^[1] due to their wide application in biosensing,^[2] and chiral catalytic,^[3] as well as photonic devices.^[4] The conformation organization of the building blocks determines the functionalities of the assemblies, especially the optical properties.^[5] There are now chiroptical nanoassemblies with helices,^[6] pyramids,^[7] scissor-like nanoparticle (NP) pairs,^[2a,8] and other superstructures,^[9] which are composed of supramolecular polymers,^[10] metal NPs,^[1b,2a,11] semiconductor NPs,^[12] carbonaceous nanomaterials,^[13] and nanocomposites.^[9c,14] Some studies have also reported propeller-like chiral structures at the molecular level for organic complexes.^[5,15] However, to date, there are no reports on propeller-like chiral assemblies at the nanoscale. Due to their scale and strong electron polarizability of inorganic compounds,^[6c,11] metal nanomaterials-mediated assemblies can give rise to intense circular dichroism (CD) at visible or near infrared wavelengths. The majority of the current research is focused on the plasmonic chiral nanomaterials.^[1b,2a,6c,11,16] Other studies have been performed on the plasmon-exciton coupling between metal nanomaterials and semiconductor NPs or chiral molecules.^[9a,12] To date, there are few reports on the chiral assembly of metal-upconversion nanostructures and their chiral mechanism is not clear, although multiparticle assemblies reporting upconversion nanoparticles (UCNPs) have been reported.^[7c,14,17]

Lanthanide-doped luminescence upconversion nanomaterials can emit higher energy light than the excitation source.^[2c]

Compared with the traditional down-conversion luminescence materials, they have a narrower band emission, longer fluorescence lifetime, and are nontoxic, which has made them promising luminescent materials in the biomedical field,^[2d,18] in areas such as biological imaging,^[19] and in cancer diagnosis and treatment.^[20] However, the conventional luminescence efficiency of lanthanide-doped luminescence upconversion nanomaterials does not exceed 1%, which restricts their widespread use in the fields of biomedical science and photonic devices.^[2c,20a,21] It is known that the plasmonic resonance coupling of metal nanomaterials can enhance the luminescence of fluorescent dyes^[1d,22] and NPs.^[23] Enhancement of UCNP light emission upon assembly with plasmonic NPs or nanorods is also possible.^[2c,21,24] However, the plasmon-enhanced upconversion luminescence has been studied for rigid solid metal supports. While this is interesting for electro-optical devices, both biological imaging and diagnostics^[2c,24d,e] require UCNP-plasmon systems to be dispersible in biological fluids, which has not been realized so far. An additional consideration regarding the significance of such systems is that optical properties of the deformable colloids involving plasmonic NPs can be strongly dependent on their geometry, which can be utilized for biomedical purposes.^[1b,2a,16,25] As we and other scientists in this field learned recently, even seemingly minor changes in the geometry of such assemblies are expected to strongly affect rotatory optical activity.^[1c,26]

In this study, we fabricated gold nanorod (NR)-UCNP tetramers in solution by adopting the DNA-driven self-assembly strategy to overcome the above-mentioned obstacles. By choosing specific building blocks—i.e., lengths of DNA sequences, aspect ratios of NRs, and sizes of UCNPs—the nanoscale engineered tetramers possessed strong and tailorable chiral activity in the visible region. Tuning the distance between the UCNP and NRs allowed us to realize the enhancement of upconversion luminescence with a 21.3-fold increase in aqueous solution. We also observed that these tetramers have propeller-like geometry that gave rise to strong chiroptical activity. In addition to having fundamental importance as an analog of propeller-like chiral molecules known from coordination chemistry, the chiral geometry of such systems makes possible the attomolar DNA detection with two-model capabilities.

Chiral tetramers were assembled from NRs and UCNPs functionalized with complementary DNA (see Experimental Section). Preferential binding of thiol-terminated DNA to the end facets of NRs allowed for end site blocking of the presynthesized NRs with a molar ratio of helper DNA to NRs of

Dr. X. Wu, Dr. L. Xu, Dr. W. Ma, Dr. L. Liu,
Prof. H. Kuang, Prof. C. Xu
State Key Lab of Food Science and Technology
Jiangnan University
Wuxi, Jiangsu 214122, P. R. China
E-mail: kuangh@jiangnan.edu.cn

Dr. X. Wu, Dr. L. Xu, Dr. W. Ma, Dr. L. Liu,
Prof. H. Kuang, Prof. C. Xu
International Joint Research Laboratory
for Biointerface and Biodection and School of Food Science
and Technology
Jiangnan University
Wuxi, Jiangsu 214122, P. R. China
Prof. N. A. Kotov
Department of Chemical Engineering
University of Michigan
Ann Arbor, MI 48109-2136, USA



DOI: 10.1002/adma.201601261

≈ 80 .^[2a,27] The subsequent addition of thiolated DNA (DNA1) led to attachment to the side facets of NRs, with a molar ratio of 1:1 for DNA1 to NRs. To protect the NRs from excessive DNA modifications and make them stable for the hybridization system, thiolated polyethylene glycol (PEG) was added to the solution at a ratio of 200 (PEG to NR-DNA1).^[2a] Simultaneously, the maleimide-PEGylated UCNPs (Yb/Er-doped NaGdF₄ NPs) were modified with the complementary thiolated DNA sequence (DNA2) due to the classic thiol-maleimide “click” reaction,^[28] and the molar ratio of DNA2 strands to UCNPs was ≈ 3 , denoted as UCNP-DNA2. To obtain the tetramers, a 33% excess of the DNA-modified NRs was intentionally maintained; the added molar ratio was fourfold that of the conjugated UCNPs. The variation in building blocks brought about the finely controlled construction of the expected NR-UCNP tetramer assemblies, denoted as AUT (Figure 1a).

To study the chiroplasmonic properties of the tetramers, 20 ± 2.7 nm UCNPs (UCNP₂₀) and a longitudinal plasmon band (λ_L) of 750 nm for NRs (average length 50.2 ± 2.1 nm and an aspect ratio of 3.3, denoted as NR₇₅₀) were used as building blocks for the nanoassemblies, with 30 base pairs (bp, about 10 nm) of DNA sequence (Figure S1 and Table S1, Supporting Information). DNA hybridization led to the formation of tetramers (AUT₇₅₀), and the corresponding NR-UCNP assemblies were identified by transmission electron microscopy (TEM, Figure 1c and Figure S2, Supporting Information) and cryo-TEM tomography (Figure 1d and Figure S3, Supporting Information). Their formation was also confirmed by dynamic light scattering measurements (DLS, Figure S4a, Supporting Information). The average hydrodynamic diameter (D_h) of the NR-UCNP tetramers was 86 ± 3.2 nm, without larger

aggregations. As a control, the DLS curve of the mixture of NRs and UCNPs was also measured, and showed a very broad peak in the range of 15–100 nm. The λ_L band of the tetramers experienced a small blue shift of about 6 nm after the assembly, whereas the transverse peak changed very little, probably due to the large distance between the NRs, which led to weak coupling of transverse plasmons (Figure 2b).^[29]

As seen from the CD spectra in Figure 2a, the tetramers revealed CD bands in the ultraviolet (UV) section of the spectrum (200–250 nm) attributed to the DNA bridges.^[6a] Concurrent with the formation of tetramers, a strong increase in chiroptical activity in the plasmonic region (300–800 nm) of the spectrum was observed (Figure 2a). In relation to other NR assemblies, the CD signal of the tetramers displayed a bisignate shape in the spectrum between the λ_L from 600 to 800 nm.^[2a,6c] The spectral “wave” for 600–750 nm was negative (-32.7 mdeg, λ_L 713 nm), and was positive for 750–800 nm (32.9 mdeg, λ_L 776 nm).^[30] A new CD peak in the 280–380 nm spectral window appeared with the assembly of tetramers, and was assigned to the absorption of UCNPs, consistent with their UV-vis spectra (Figure 2b). The chiral anisotropy factor, g , of the assembled tetramers reached 1.06×10^{-2} . As a comparison, the DNA-conjugated NRs and UCNPs showed strong chiroptical activity in the UV region (200–250 nm). However, all the tested permutations of modified and unmodified starting NPs (NRs and UCNPs), exhibited weak CD, if any, bands at 250–800 nm, in agreement with previous reports (Figure 2a).^[8,31]

In order to better understand the mechanism of rotatory optical activity of the NR-UCNP assemblies, tetramers with their various geometries and various constituent building blocks were assembled. Taking into consideration that plasmonic

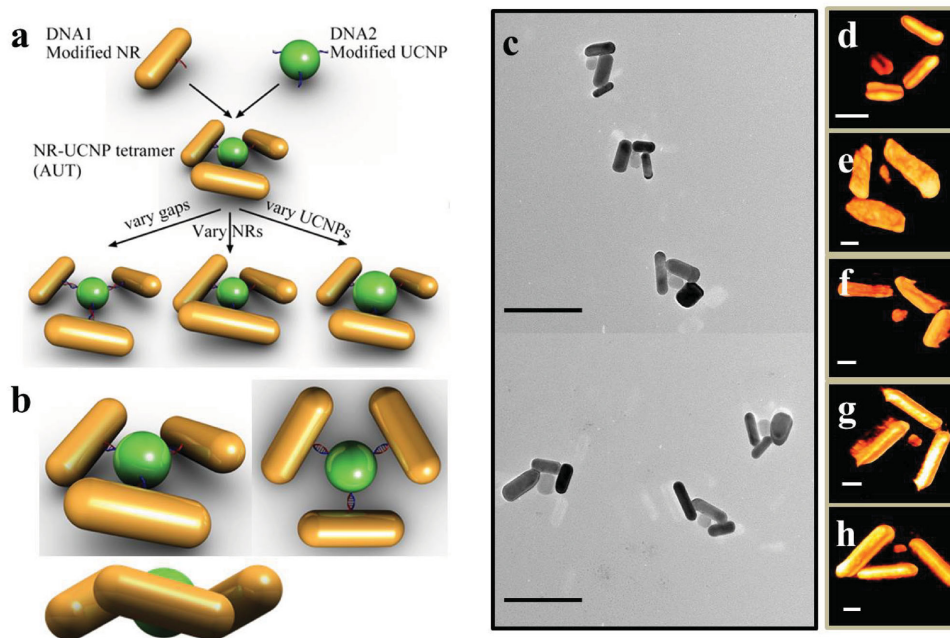


Figure 1. Structural characteristics of NR-UCNP tetramer assemblies (AUT). a) Schematic illustration for the assembly. b) The geometric structure illustrations of the tetramer. The illustrations are the front view (upper left), top view (upper right), and the side view (lower left), respectively. Representative c) TEM images and d–h) cryo-TEM tomographic reconstructions of NR-UCNP tetramer assembly. The different longitudinal absorption peak of NR was c,d) 750 nm, e) 700 nm; f) 800 nm; g) 850 nm; and h) 900 nm, respectively; scale bar in c) and d–h) is 100 and 20 nm, respectively.

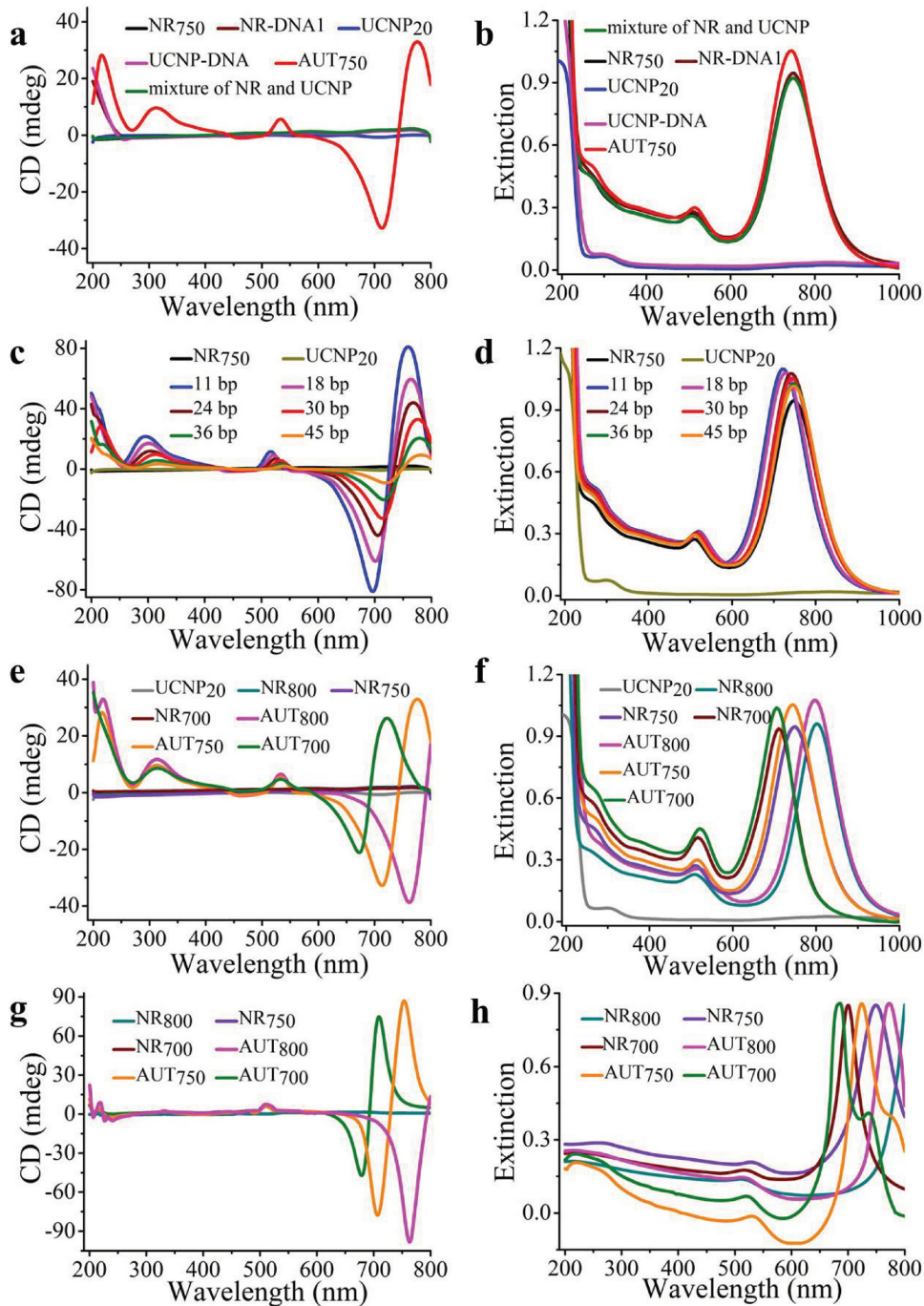


Figure 2. Chiroptical activities of the NR-UCNP tetramer assemblies. a,c,e) The experimental CD and b,d,f) UV-vis extinction spectra for NR-UCNP tetramer assembly with different lengths of c,d) DNA sequences, and e,f) different longitudinal absorption of NRs and a,b) their controls. The g) theoretical CD and h) UV-vis extinction spectra of NR-UCNP tetramer and their starting NRs. The NR-UCNP tetramers were assembled with 30 bp of DNA sequence, 20 nm of UCNP, and the longitudinal absorption peak of NR of 700, 750, and 800 nm.

coupling strongly depends on the distance between the plasmonic particles,^[32] we first studied the chiral optical activity of the tetramers assembled with varying lengths of DNA sequence (11, 18, 24, 30, 36, 45 bp). From the spectral measurements in Figure 2c, all the CD curves possessed similar spectral waves, with a bisignate signal for plasmonic bands at 600–800 nm. As the DNA length decreased from 45 to 11 bp, the λ_L of the

CD bands significantly shifted to blue by 23 and 22 nm for the positive and negative part, respectively. This blue-shift of the CD spectra was in good agreement with the UV-vis spectra, although the latter showed a smaller blue shift (about 18 nm, Figure 2d). Synchronously, CD signals showed a progressive increase in amplitude from +9.3 to +80.9 mdeg along with a shorter DNA sequence. The g -factor value reached 2.1×10^{-2} ,

which was much higher than the molecular system (10^{-3} – 10^{-5}) and comparable to the highest obtained for NP assemblies reported so far.^[8,33]

In addition to alterations in the length of the DNA strands, NRs with different λ_L absorption were also investigated. Another two sets of NRs, with λ_L absorption of 700 nm (aspect ratio of 2.6) and 800 nm (aspect ratio of 3.7), were also chosen for tetramer assembly. These tetramers were denoted as AUT₇₀₀ and AUT₈₀₀, respectively (Figure 1e,f and S5–S8, Supporting Information). The average D_h value of the tetramers increased from 75.3 ± 2.1 to 101 ± 6.7 nm as the λ_L absorption increased from 700 to 800 nm (Figure S4b, Supporting Information). This change in D_h correlated with the statistical size measurements from the TEM images (Figures S5 and S6, Supporting Information). A strong chiroplasmonic response was observed with varying λ_L absorption of starting NRs. The plasmonic CD spectra displayed a marked red shift (89 nm, at the negative peak), corresponding to that of the absorption changes (Figure 2e,f). Increased λ_L of starting NRs (from 700 to 800 nm) led to stronger CD intensity, with an absolute CD value from 21.2 to 38.7 mdeg. These results demonstrate that chiroptical tetramers can be constructed and engineered by adjustment of the DNA sequence and plasmonic absorption of NRs, and the largest g-factor value occurred at tetramer with 11 bp of the DNA sequence, λ_L absorption of 750 nm of the NRs, and 20 nm UCNP.

The 3D reconstruction of TEM tomography revealed that the three constitutive NRs in the tetramer were not parallel to each other, but had propeller-like conformations, which was likely due to the balancing of electrostatic attraction and repulsion forces, similar to many other nanoscale assemblies with biopolymers.^[5,8,15d,34] As expected, such geometry of the tetramers was not superimposable with their mirror images (Figure 1b,d–h; Figures S3, S7–S9, Supporting Information), which resulted in strong chiroptical activity.^[15a,c] Similarly to the case of other chiral NPs or NRs assemblies triggered by biomolecules,^[2a,8,26a] the strong chiroptical activity of propeller-like NR-UCNP tetramers was a difference of two types of enantiomers. The preference for one enantiomer as opposed to another was related to connecting DNA bridges and the general preference of charged nanoscale NRs as the conformation with minimal energy.^[2a,26a]

To further understand the origin of the tetramer's chirality, chiroptical simulations were carried out based on the frequency domain finite integral (FDFI) method, with 20 nm UCNP and a 10 nm gap between the NRs and UCNP. The length of the NRs was set to 50.2 nm, and the aspect ratio was 2.6, 3.3, and 3.7, respectively (Figure 2g,h). The simulated UV–vis spectra of the tetramers showed obvious blue-shift (15, 24, and 27 nm) compared with the original NRs (NR₇₀₀, NR₇₅₀, NR₈₀₀; Figure 2h), which was consistent with the experimental spectra (Figure 2f). The calculated CD curve exhibited a predicted bisignate signature in the 600–800 nm region (Figure 2g), which correlated with the λ_L chiral absorption of NRs as observed experimentally (Figure 2e).

Based on the above test results, the chiral optical activity of NR-UCNP tetramers was attributed to the unique propeller-like geometry of the assemblies (Figure 1b,d–h; Figures S3 and S7–S9, Supporting Information), and was confirmed by theoretical

simulation (Figure 2g). In addition, it must be pointed out that other factors should be considered including plasmon–plasmon coupling of the NRs.^[6a,35] The induced plasmonic CD originating from the electronic “imprint” of the DNA helix on electronic oscillations is likely to play a minor role based on previous studies.^[26a,36] It should also be pointed out that the propeller-like geometry creates a strong plasmonic field, resulting in the appearance of chiroptical bands in UCNP (Figure 2a,c,e), which is unusual for these NPs and certainly worthy of further study.

In addition to the chiroptical activity of the NR-UCNP tetramers, the luminescence of the assemblies was investigated. The AUT₇₅₀ tetramer made from UCNP₂₀, NR₇₅₀, and 30 bp of DNA, was used as the initial model. Under 980 nm laser excitation, up-conversion luminescence (UCL) of Yb/Er-doped UCNP was observed with the typical emission peaks located at 529, 546, and 662 nm, which were attributed to the electronic transitions in Er³⁺ from ²H_{11/2} and ⁴S_{3/2} states to the ⁴I_{15/2} state, and from the ⁴F_{9/2} state to the ⁴I_{15/2} state.^[28] The intensity of UCL gradually increased in the first 75 min as tetramers assembled matching the typical timing of DNA hybridization (Figure 3). In the following 60 min of the experiment, the intensity was unchanged.

The luminescence enhancement due to the formation of tetramers can be shown as I/I_0 , where I_0 and I represent the UCL intensity observed for original UCNP and assembled tetramers, respectively. The UCL enhancement factors of the tetramers were 3.8, 5.3, and 6.6 for the emission bands at 529, 546, and 662 nm, respectively (Figure 3g). In a control experiment, which indicated the significance of the assembly for UCL enhancement, we determined the change in UCL intensity after DNA modification when mixed with the NR dispersion. Without DNA bridges and tetramer formation, UCL peaks showed a slight decrease (Figure 3b). We also considered the possibility of UCL fluctuation due to the buffer conditions and pH value of the assembly system. As seen in Figure S10 (Supporting Information), there was no obvious variation in UCL in the tested buffer conditions and pH range 7.0 to 8.5, consistent with the related D_h and electrokinetic potentials measurements (Figure S4c, Supporting Information).

To evaluate the influence of distance from the surface of NRs to UCNP on the UCL spectra, AUT₇₅₀ tetramers were assembled with different DNA strand lengths (11, 18, 24, 30, 36, and 45 bp). The UCL signal was strongly quenched when the DNA sequence was shorter than 18 bp, especially with a short DNA sequence of 11 bp. The UCL quenching was ascribed to the nonradiative energy transfer (NRET) to plasmonic states in gold.^[17,23] When the distance between the NRs and NPs increased, i.e., DNA length increased to 24 and 36 bp, UCL enhancement compared with that of starting UCNP was observed (Figure 3c). The maximum enhancement of UCL was obtained at 30 bp, after which the UCL intensity decreased to that of the original UCNP due to low electric field intensity induced by the excess distance.^[2c]

When NR₇₅₀ were replaced with NR₉₀₀ (Figure 3d), the strongest UCL was also obtained for 30 bp DNA bridges. The maximum enhancement factor of the assembled AUT₉₀₀ tetramers was up to 8.5 and 12.4 at the bands of 529 and 546 nm, respectively (Figure 3g). For the band at 662 nm, the UCL

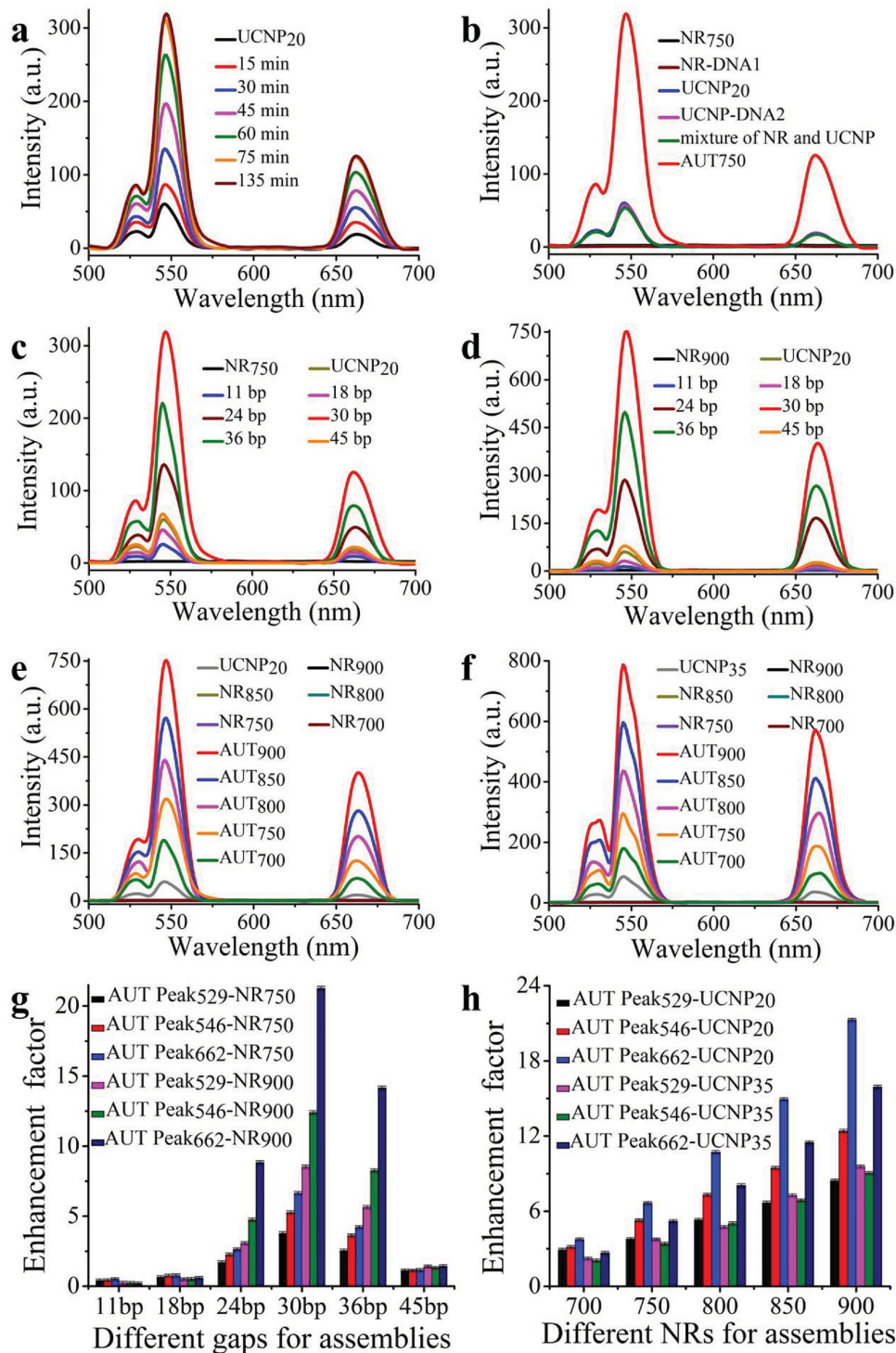


Figure 3. Up-conversion luminescence spectra of the NR-UCNP tetramer assembly and their controls under excitation at 980 nm. a) Dynamic luminescence spectra for the assembly. b) Luminescent spectra of NR-UCNP tetramers and their controls. Assembly with different lengths of DNA sequences with the longitudinal absorption peak of NRs of c) 750 nm, and d) 900 nm. Assembly with different NRs, where UCNP was e) 20 nm, and f) 35 nm. Luminescent enhancement factor curves of g) c, d, and h) e, f.

of AUT₉₀₀ tetramers was 21.3-fold enhanced compared with the original UCNP, which was approximately 3.3 times higher than the UCL of AUT₇₅₀ tetramers at the same band (Figure 3g).

Further experiments were carried out to reveal the relationship between the UCL signal and the λ_L absorption (700, 750, 800, 850, and 900 nm) of tetramers. The UCL intensity progressively increased with increasing λ_L absorption (700–900 nm),

with a corresponding enhancement factor of 2.9, 3.8, 5.3, 6.7, and 8.5 at 529 nm, 3.1, 5.3, 7.3, 9.5, and 12.4 at 546 nm, and 3.7, 6.6, 10.7, 15.0, and 21.3 at 662 nm, respectively (Figure 3e,h). In these experiments, optimized enhancement was with AUT₉₀₀, probably due to the closer proximity to the excitation wavelength of UCNP (980 nm) for λ_L absorption of AUT₉₀₀ compared to the others.^[17]

Dependence of the UCL intensity on plasmonic resonance was further confirmed by the tetramers assembled with larger UCNP with a diameter of 35 ± 2.2 nm (UCNP₃₅). The influence of varied λ_L absorption of NRs (700, 750, 800, 850, and 900 nm) on UCL was investigated based on the AUT tetramers established by UCNP₃₅ and a DNA sequence of 30 bp. As shown in Figure 3f,h, the UCL enhancement factor was 2.2, 3.7, 4.7, 7.2, and 9.6 at 529 nm, and 2.1, 3.4, 5.0, 6.9, and 9.1 at 546 nm; whereas at 662 nm, the enhancement factor was 2.7, 5.2, 8.1, 11.5, and 16.0, respectively. These were all smaller in the case of tetramers comprising UCNP₂₀, indicating that the plasmonic-UCL enhancement was better for smaller sized UCNP.

Here, it was clearly revealed that the maximum UCL enhancement factor occurred at a distance of ≈ 10 nm (30 bp of the DNA sequence), λ_L absorption of 900 nm of the NRs, and 20 nm UCNP in the tested tetramers. To the best of our

knowledge, this is the first time that plasmon-enhanced UCL has been successfully achieved in solution. Plasmon enhancement of UCL is ascribed to two effects: (1) increased excitation rate and efficiency arising from localized electric field enhancement by the collective oscillation coupling of NRs in the tetramers;^[17,24e] and (2) enhanced radiative decay rate and effective emission induced by the UCL emission coupling with plasmon resonance of NRs.^[23,24d,37] Electromagnetic simulations were performed to further confirm the UCL enhancement. The electric field of the AUT₇₅₀ patterns assembled with 20 nm UCNP, were calculated for three representative distances (3.7, 10, 15 nm) from the surface of the UCNP to NRs. As shown in Figure 4a–c, the electric field intensity of the tetramers gradually decreased with increasing distance (6.51 V m⁻¹ for a 3.7 nm gap, 5.86 V m⁻¹ for a 10 nm gap, 5.34 V m⁻¹ for a 15 nm gap), corresponding to the larger UCL enhancement factor of tetramers with a gap of 10 nm (5.3-fold at 546 nm) than a gap of 15 nm (1.1-fold at 546 nm) (Figure 3g). In contrast, as the distance approached 3.7 nm, the NRET (declined with inverse fourth power of localized electric field^[17,24a]) overwhelmingly dominated,^[1d] therefore the UCL intensity was significantly quenched, although with a higher electric field than the above two cases. When the distance of AUT₇₅₀ was set at 10 nm, the tetramers constructed with 35 nm UCNP showed lower

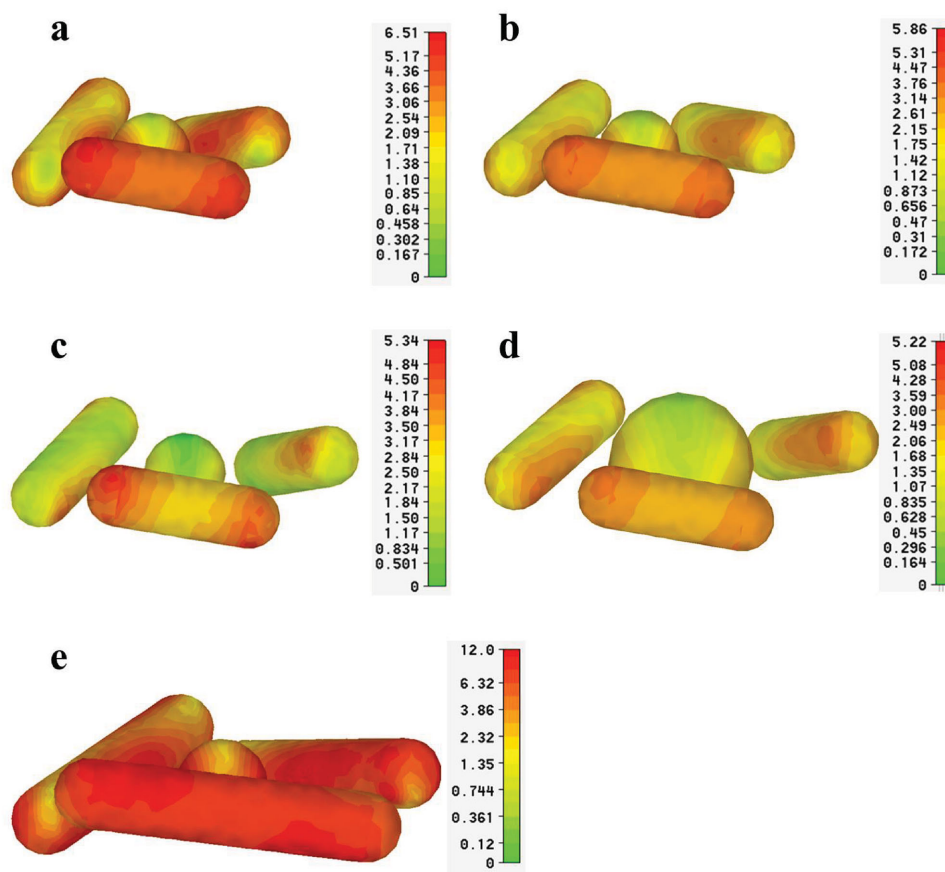


Figure 4. The electromagnetic simulations of the NR-UCNP tetramer. a,b,c) The electric field of NR-UCNP tetramer assembled with a) 11 bp, b) 30 bp, and c) 45 bp of DNA sequences, where the longitudinal absorption peak of NR was 750 nm, and the size of UCNP was 20 nm. d) The electric field of NR-UCNP tetramer assembled with 30 bp of DNA sequence, the longitudinal absorption peak of NR of 750 nm, and 35 nm of UCNP. e) The electric field of NR-UCNP tetramer assembled with 30 bp of DNA sequence, the longitudinal absorption peak of NR of 900 nm, and 20 nm of UCNP.

electric field intensity (5.22 V m^{-1}) than the tetramers built with 20 nm UCNPs, producing a smaller UCL enhancement factor (Figures 3h, 4d). When the distance of the tetramers and the size of UCNPs were set at 10 nm and 20 nm, the AUT_{900} possessed a higher electric field (12.0 V m^{-1}) and thus resulted in stronger UCL than AUT_{750} (Figures 3g, 4e).

Strong chiroptical and luminescent activity of the propeller-like assemblies enabled two-model biosensing of oligonucleotides, which improved the reliability and versatility of the method. Hepatitis A virus *Vall7* polyprotein gene (*HVA*) was selected as the target.^[38] As illustrated in Figure 5a, NR-UCNP tetramers were fabricated with two partly complementary DNA sequences (Table S1, Supporting Information), by forming hairpin-like DNA structures between NR and UCNP. In the presence of oligonucleotide targets, hairpin-like DNA strands of the tetramers were extended, due to their specific biorecognition; and resulted in a longer gap length, which caused the reduction of both UCL and CD signal intensities. In the case

of the chiroplasmonic method, AUT_{750} was adopted, and the calibration curve was obtained with a difference in CD intensity ($\text{CD}_{776 \text{ nm}} - \text{CD}_{713 \text{ nm}}$) (Figure 5b,c). It exhibited an excellent linear response to the DNA target over the range of 3.3×10^{-8} to $3.3 \times 10^{-5} \text{ nM}$. The limit of detection (LOD) was found to be 13.2 aM (Figure 5c, see Supporting Information for details). The UCL method was carried out using AUT_{750} (Figure 5d). The standard curve was plotted with the UCL peak intensity at 546 nm as the y axis, and the logarithmic DNA concentration as the x axis. As shown in Figure 5e, the obtained LOD of 20.3 aM was almost two times higher than that of the CD technique with the AUT_{750} assemblies, which was attributed to strong polarization rotation by the propeller-like geometry of the plasmonic nanoassemblies and bisignate characteristic of the CD spectra.^[2a,8] As a control, AUT_{900} tetramers can also be used as a luminescence biosensor (Figure S11, Supporting Information). Besides confirming the sensitivity, we evaluated the specificity of the developed method, by using non-complementary

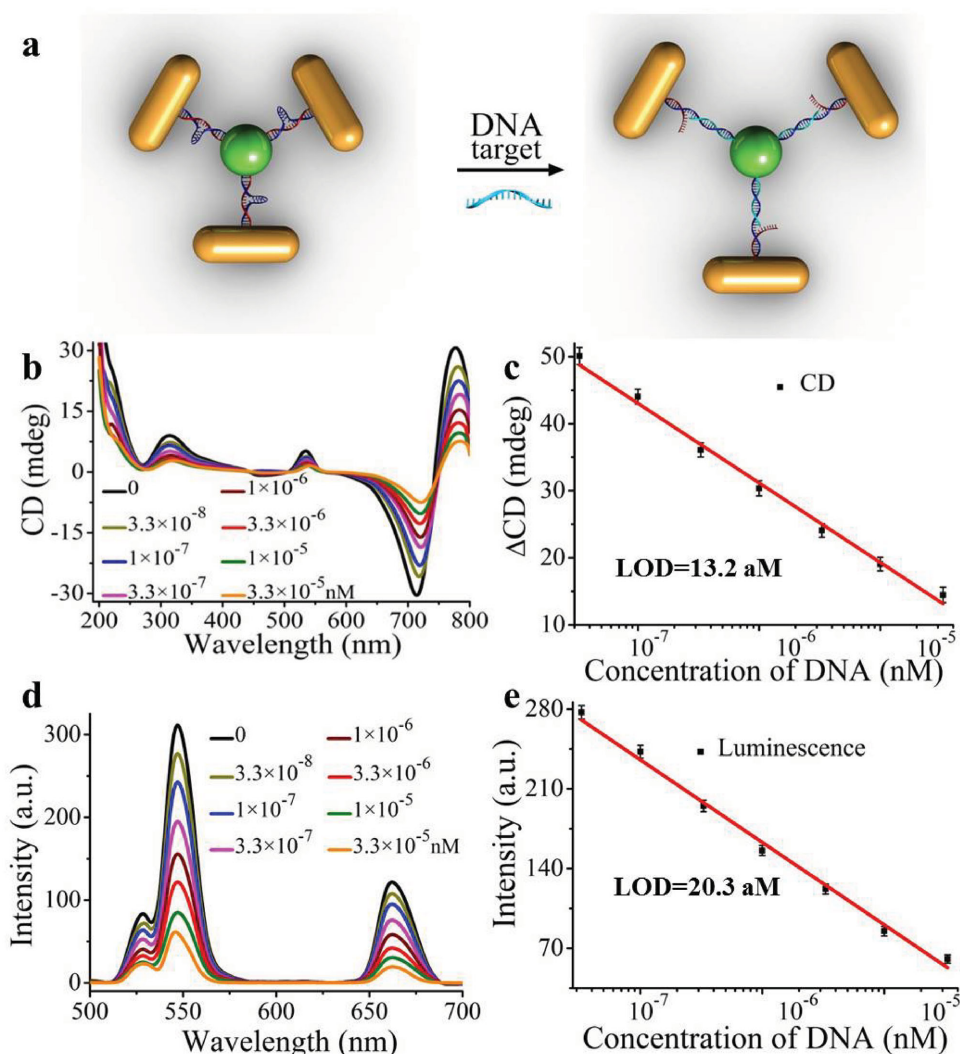


Figure 5. DNA detection by up-conversion luminescent and chiroplasmonic techniques with the NR-UCNP tetramer assembly. a) Schematic illustration for the DNA biosensing. b) The CD and d) up-conversion luminescence curves with increasing concentrations of DNA solution. c) The CD and e) up-conversion luminescent calibration curves for DNA detection. The longitudinal absorption peak of NR using for assembly was 750 nm.

hybridization DNA sequences as negative controls. The results (Figure S12, Supporting Information) showed that no obvious changes of CD signal or luminescence was observed, indicating good specificity of the biosensor. Furthermore, we also evaluated the practical application of the developed biosensor in a complex biological matrix, such as human serum. The results in Table S2 (Supporting Information) demonstrated excellent recoveries of analyte by the biosensor. In comparison with other conventional methods (such as ELISA, HPLC, plasmon resonance shift assay), therefore, the developed method possessed better sensitivity and signal-to-noise ratio, as well as more accurate quantitative determination. In addition, dual signal-detection model of the method enabled the accurate and distinct identification of cancer biomarkers, which holds promising potential for early disease diagnosis.

In summary, these propeller-like nanoscale tetramers not only offer strong chiroplasmonic and enhanced upconversion luminescent properties, but also enable DNA detection with an unusually low LOD. Looking forward, the UCNPs-based chiroplasmonic assemblies show potential for efficient bioimaging and light-guided therapy *in vitro* and *in vivo*. In addition, the ultrasensitive bioanalysis nanoplatform may also satisfy the urgent requirements for early medical diagnosis, environmental monitoring, anti-counterfeiting, and fingerprint forensics.

Supporting Information

Supporting Information is available from the Wiley Online Library or from the author.

Acknowledgements

X.W. and L.X. contributed equally to this paper. This work is financially supported by the National Natural Science Foundation of China (21471068, 31400848, 21471128, 21522102, 21503095).

Received: March 4, 2016

Revised: April 5, 2016

Published online: May 9, 2016

- [1] a) J. Yeom, B. Yeom, H. Chan, K. W. Smith, S. Dominguez-Medina, J. H. Bahng, G. Zhao, W.-S. Chang, S.-J. Chang, A. Chuvilin, D. Melnikau, A. L. Rogach, P. Zhang, S. Link, P. Král, N. A. Kotov, *Nat. Mater.* **2015**, *14*, 66; b) R. Schreiber, N. Luong, Z. Fan, A. Kuzyk, P. C. Nickels, T. Zhang, D. M. Smith, B. Yurke, W. Kuang, A. O. Govorov, T. Liedl, *Nat. Commun.* **2013**, *4*, 2948; c) S. Ostovar pour, L. Rocks, K. Faulds, D. Graham, V. Parchaňský, P. Bouř, E. W. Blanch, *Nat. Chem.* **2015**, *7*, 591; d) G. P. Acuna, F. M. Möller, P. Holzmeister, S. Beater, B. Lalkens, P. Tinnefeld, *Science* **2012**, *338*, 506.
- [2] a) W. Ma, H. Kuang, L. Xu, L. Ding, C. Xu, L. Wang, N. A. Kotov, *Nat. Commun.* **2013**, *4*, 2689; b) Z. Li, Z. Zhu, W. Liu, Y. Zhou, B. Han, Y. Gao, Z. Tang, *J. Am. Chem. Soc.* **2012**, *134*, 3322; c) J. Zhou, Q. Liu, W. Feng, Y. Sun, F. Li, *Chem. Rev.* **2015**, *115*, 395; d) W. Zheng, P. Huang, D. Tu, E. Ma, H. Zhu, X. Chen, *Chem. Soc. Rev.* **2015**, *44*, 1379.
- [3] a) K. V. S. Ranganath, J. Kloesges, A. H. Schäfer, F. Glorius, *Angew. Chem. Int. Ed.* **2010**, *49*, 7786; b) K. Sawai, R. Tatum, T. Nakahodo, H. Fujihara, *Angew. Chem. Int. Ed.* **2008**, *47*, 6917.
- [4] a) G. Chen, H. Agren, T. Y. Ohulchanskyy, P. N. Prasad, *Chem. Soc. Rev.* **2015**, *44*, 1680; b) X. Li, F. Zhang, D. Zhao, *Chem. Soc. Rev.* **2015**, *44*, 1346.
- [5] T. Nakano, Y. Okamoto, *Chem. Rev.* **2001**, *101*, 4013.
- [6] a) A. Kuzyk, R. Schreiber, Z. Fan, G. Pardatscher, E.-M. Roller, A. Högele, F. C. Simmel, A. O. Govorov, T. Liedl, *Nature* **2012**, *483*, 311; b) G. Singh, H. Chan, A. Baskin, E. Gelman, N. Reppin, P. Král, R. Klajn, *Science* **2014**, *345*, 1149; c) X. Lan, X. Lu, C. Shen, Y. Ke, W. Ni, Q. Wang, *J. Am. Chem. Soc.* **2015**, *137*, 457.
- [7] a) W. Yan, L. Xu, C. Xu, W. Ma, H. Kuang, L. Wang, N. A. Kotov, *J. Am. Chem. Soc.* **2012**, *134*, 15114; b) A. J. Mastroianni, S. A. Claridge, A. P. Alivisatos, *J. Am. Chem. Soc.* **2009**, *131*, 8455; c) S. Li, L. Xu, W. Ma, X. Wu, M. Sun, H. Kuang, L. Wang, N. A. Kotov, C. Xu, *J. Am. Chem. Soc.* **2016**, *138*, 306.
- [8] X. Wu, L. Xu, L. Liu, W. Ma, H. Yin, H. Kuang, L. Wang, C. Xu, N. A. Kotov, *J. Am. Chem. Soc.* **2013**, *135*, 18629.
- [9] a) Z. Zhu, J. Guo, W. Liu, Z. Li, B. Han, W. Zhang, Z. Tang, *Angew. Chem.* **2013**, *125*, 13816; b) C. Tan, X. Qi, Z. Liu, F. Zhao, H. Li, X. Huang, L. Shi, B. Zheng, X. Zhang, L. Xie, Z. Tang, W. Huang, H. Zhang, *J. Am. Chem. Soc.* **2015**, *137*, 1565; c) W. Liu, Z. Zhu, K. Deng, Z. Li, Y. Zhou, H. Qiu, Y. Gao, S. Che, Z. Tang, *J. Am. Chem. Soc.* **2013**, *135*, 9659; d) C. Hao, L. Xu, W. Ma, X. Wu, L. Wang, H. Kuang, C. Xu, *Adv. Funct. Mater.* **2015**, *25*, 5816.
- [10] L. Zhang, L. Qin, X. Wang, H. Cao, M. Liu, *Adv. Mater.* **2014**, *26*, 6959.
- [11] S. H. Jung, J. Jeon, H. Kim, J. Jaworski, J. H. Jung, *J. Am. Chem. Soc.* **2014**, *136*, 6446.
- [12] A. Ben-Moshe, B. M. Maoz, A. O. Govorov, G. Markovich, *Chem. Soc. Rev.* **2013**, *42*, 7028.
- [13] P. Deria, C. D. Von Barga, J.-H. Olivier, A. S. Kumbhar, J. G. Saven, M. J. Therien, *J. Am. Chem. Soc.* **2013**, *135*, 16220.
- [14] L.-L. Li, Y. Lu, *J. Am. Chem. Soc.* **2015**, *137*, 5272.
- [15] a) F. Vera, R. M. Tejedor, P. Romero, J. Barberá, M. B. Ros, J. L. Serrano, T. Sierra, *Angew. Chem.* **2007**, *119*, 1905; b) J. Barberá, L. Puig, P. Romero, J. L. Serrano, T. Sierra, *J. Am. Chem. Soc.* **2006**, *128*, 4487; c) A. Martinez, L. Guy, J.-P. Dutasta, *J. Am. Chem. Soc.* **2010**, *132*, 16733; d) F. Grillo, V. Mugnaini, M. Oliveros, S. M. Francis, D.-J. Choi, M. V. Rastei, L. Limot, C. Cepek, M. Pedio, S. T. Bromley, *J. Phys. Chem. Lett.* **2012**, *3*, 1559.
- [16] X. Shen, A. Asenjo-Garcia, Q. Liu, Q. Jiang, F. J. García de Abajo, N. Liu, B. Ding, *Nano Lett.* **2013**, *13*, 2128.
- [17] A. L. Feng, M. L. You, L. Tian, S. Singamaneni, M. Liu, Z. Duan, T. J. Lu, F. Xu, M. Lin, *Sci. Rep.* **2015**, *5*, 7779.
- [18] a) Y. I. Park, K. T. Lee, Y. D. Suh, T. Hyeon, *Chem. Soc. Rev.* **2015**, *44*, 1302; b) X. Liu, C.-H. Yan, J. A. Capobianco, *Chem. Soc. Rev.* **2015**, *44*, 1299; c) B. Zhou, B. Shi, D. Jin, X. Liu, *Nat. Nanotechnol.* **2015**, *10*, 924; d) X. Zhao, L. Xu, M. Sun, W. Ma, X. Wu, H. Kuang, L. Wang, C. Xu, *Small* **2016**, DOI: 10.1002/smll.201503629.
- [19] a) J.-N. Liu, W.-B. Bu, J.-L. Shi, *Acc. Chem. Res.* **2015**, *48*, 1797; b) R. Deng, F. Qin, R. Chen, W. Huang, M. Hong, X. Liu, *Nat. Nanotechnol.* **2015**, *10*, 237; c) R. Li, Z. Ji, J. Dong, C. H. Chang, X. Wang, B. Sun, M. Wang, Y.-P. Liao, J. I. Zink, A. E. Nel, T. Xia, *ACS Nano* **2015**, *9*, 3293.
- [20] a) G. Chen, H. Qiu, P. N. Prasad, X. Chen, *Chem. Rev.* **2014**, *114*, 5161; b) D. Yang, P. a. Ma, Z. Hou, Z. Cheng, C. Li, J. Lin, *Chem. Soc. Rev.* **2015**, *44*, 1416; c) H. Dong, S.-R. Du, X.-Y. Zheng, G.-M. Lyu, L.-D. Sun, L.-D. Li, P.-Z. Zhang, C. Zhang, C.-H. Yan, *Chem. Rev.* **2015**, *115*, 10725; d) L. Cheng, C. Wang, L. Feng,

- K. Yang, Z. Liu, *Chem. Rev.* **2014**, *114*, 10869; e) M. Sun, L. Xu, W. Ma, X. Wu, H. Kuang, L. Wang, C. Xu, *Adv. Mater.* **2016**, *28*, 898.
- [21] L.-D. Sun, Y.-F. Wang, C.-H. Yan, *Acc. Chem. Res.* **2014**, *47*, 1001.
- [22] a) H. Yuan, S. Khatua, P. Zijlstra, M. Yorulmaz, M. Orrit, *Angew. Chem. Int. Ed.* **2013**, *52*, 1217; b) S. Khatua, P. M. R. Paulo, H. Yuan, A. Gupta, P. Zijlstra, M. Orrit, *ACS Nano* **2014**, *8*, 4440; c) A. Kinkhabwala, Z. Yu, S. Fan, Y. Avlasevich, K. Mullen, W. E. Moerner, *Nat. Photonics* **2009**, *3*, 654; d) P. Holzmeister, E. Pibiri, J. J. Schmied, T. Sen, G. P. Acuna, P. Tinnefeld, *Nat. Commun.* **2014**, *5*, 5356; e) A. Bek, R. Jansen, M. Ringler, S. Mayilo, T. A. Klar, J. Feldmann, *Nano Lett.* **2008**, *8*, 485.
- [23] Y. Wang, T. Yang, M. T. Tuominen, M. Achermann, *Phys. Rev. Lett.* **2009**, *102*, 163001.
- [24] a) W. Park, D. Lu, S. Ahn, *Chem. Soc. Rev.* **2015**, *44*, 2940; b) M. Saboktakin, X. Ye, U. K. Chettiar, N. Engheta, C. B. Murray, C. R. Kagan, *ACS Nano* **2013**, *7*, 7186; c) W. Zhang, F. Ding, S. Y. Chou, *Adv. Opt. Mater.* **2012**, *24*, 236; d) M. Saboktakin, X. Ye, S. J. Oh, S.-H. Hong, A. T. Fafarman, U. K. Chettiar, N. Engheta, C. B. Murray, C. R. Kagan, *ACS Nano* **2012**, *6*, 8758; e) Q.-C. Sun, H. Munderoor, J. C. Ribot, V. Singh, I. I. Smalyukh, P. Nappal, *Nano Lett.* **2014**, *14*, 101.
- [25] A. Kuzyk, R. Schreiber, H. Zhang, A. O. Govorov, T. Liedl, N. Liu, *Nat. Mater.* **2014**, *13*, 862.
- [26] a) W. Ma, H. Kuang, L. Wang, L. Xu, W.-S. Chang, H. Zhang, M. Sun, Y. Zhu, Y. Zhao, L. Liu, C. Xu, S. Link, N. A. Kotov, *Sci. Rep.* **2013**, *3*, 1934; b) C. Zhou, X. Duan, N. Liu, *Nat. Commun.* **2015**, *6*, 8102.
- [27] L. Xu, H. Kuang, C. Xu, W. Ma, L. Wang, N. A. Kotov, *J. Am. Chem. Soc.* **2012**, *134*, 1699.
- [28] R. Qiao, C. Liu, M. Liu, H. Hu, C. Liu, Y. Hou, K. Wu, Y. Lin, J. Liang, M. Gao, *ACS Nano* **2015**, *9*, 2120.
- [29] P. K. Jain, S. Eustis, M. A. El-Sayed, *J. Phys. Chem. B* **2006**, *110*, 18243.
- [30] N. Berova, L. D. Bari, G. Pescitelli, *Chem. Soc. Rev.* **2007**, *36*, 914.
- [31] I. Lieberman, G. Shemer, T. Fried, E. M. Kosower, G. Markovich, *Angew. Chem. Int. Ed.* **2008**, *47*, 4855.
- [32] a) L. Xu, W. Yan, W. Ma, H. Kuang, X. Wu, L. Liu, Y. Zhao, L. Wang, C. Xu, *Adv. Mater.* **2015**, *27*, 1706; b) K. L. Young, M. B. Ross, M. G. Blaber, M. Rycenga, M. R. Jones, C. Zhang, A. J. Senesi, B. Lee, G. C. Schatz, C. A. Mirkin, *Adv. Mater.* **2014**, *26*, 653.
- [33] B. Yeom, H. Zhang, H. Zhang, J. I. Park, K. Kim, A. O. Govorov, N. A. Kotov, *Nano Lett.* **2013**, *13*, 5277.
- [34] a) T. Gibaud, E. Barry, M. J. Zakhary, M. Henglin, A. Ward, Y. Yang, C. Berciu, R. Oldenbourg, M. F. Hagan, D. Nicastro, R. B. Meyer, Z. Dogic, *Nature* **2012**, *481*, 348; b) H. Miyake, H. Tsukube, *Chem. Soc. Rev.* **2012**, *41*, 6977; c) M. Caricato, A. K. Sharma, C. Coluccini, D. Pasini, *Nanoscale* **2014**, *6*, 7165; d) M. Caricato, A. Delforge, D. Bonifazi, D. Dondi, A. Mazzanti, D. Pasini, *Org. Biomol. Chem.* **2015**, *13*, 3593.
- [35] Y. Zhao, L. Xu, W. Ma, L. Wang, H. Kuang, C. Xu, N. A. Kotov, *Nano Lett.* **2014**, *14*, 3908.
- [36] a) X. Wu, L. Xu, W. Ma, L. Liu, H. Kuang, W. Yan, L. Wang, C. Xu, *Adv. Funct. Mater.* **2015**, *25*, 850; b) F. Lu, Y. Tian, M. Liu, D. Su, H. Zhang, A. O. Govorov, O. Gang, *Nano Lett.* **2013**, *13*, 3145.
- [37] A. Rose, T. B. Hoang, F. McGuire, J. J. Mock, C. Ciraci, D. R. Smith, M. H. Mikkelsen, *Nano Lett.* **2014**, *14*, 4797.
- [38] Y. W. C. Cao, R. Jin, C. A. Mirkin, *Science* **2002**, *297*, 1536.